Deep Unfolding-Based Sensing-Assisted Channel Estimation With Imperfect Radar Arrays

Jiapan Yang, Bo Ai, *Fellow, IEEE*, Wei Chen, *Senior Member, IEEE*,
Songjie Yang, Ning Wang, *Member, IEEE*, Chau Yuen, *Fellow, IEEE*

***Abstract*—In vehicle-to-everything (V2X) scenarios, the high dynamic characteristics of V2X environments impose significant challenges on communication channel estimation, where the emerging integrated sensing and communication technology could serve as a vital tool for achieving accurate channel estimation. This paper leverages radar-sensed angle information to assist in communication channel estimation and proposes a deep unfolding-based radar-assisted channel estimation network (Radar-CEnet). Specifically, for the radar module, to address the challenges posed by insufficient data in imperfect arrays, we employ a model-agnostic meta-learning with a convolutional neural network (MAML-CNN) approach to achieve high-precision direction-of-arrival (DOA) estimation. Then, the angle information obtained by the radar module, as prior knowledge, is used for channel estimation. Building on this, we design a novel soft-thresholding shrinkage function and propose the Radar-CEnet algorithm to efficiently estimate the sparse channel. Finally, we rigorously prove the convergence of the Radar-CEnet algorithm and demonstrate that it achieves a lower estimation error. Experimental results show that the proposed Radar-CEnet outperforms existing traditional methods and deep learning-based approaches in channel estimation performance. At an SNR of 20dB, the proposed Radar-CEnet method reduces the NMSE from –23.75dB to –27.15dB compared to the learning-based iterative soft-thresholding method, achieving an estimation accuracy improvement of approximately 54%.**

***Index Terms*—Meta-learning, deep unfolding, imperfect arrays, channel estimation.**

I. Introduction

With the rapid development of intelligent transportation systems (ITS) and autonomous driving technology, vehicle-to-everything (V2X) technology has become a fundamental pillar supporting future intelligent transportation [2]. V2X technology improves traffic safety and travel efficiency through information exchange from vehicle to vehicle (V2V), vehicle to infrastructure (V2I), and vehicles to pedestrians (V2P). As a key application scenario of ITS, integrated sensing and communication (ISAC) technology is expected to play a significant role in 6G V2X communication [3], [4]. By integrating environmental sensing and efficient communication functions into a single system, ISAC can significantly enhance spectrum utilization efficiency, reduce equipment redundancy, and improve overall system performance.

Millimeter-wave (mmWave) massive multiple-input multiple-output (MIMO) technology is a key technology for achieving high data rates and low-latency V2X communications [5]. However, the large number of antennas in mmWave massive MIMO systems increases the complexity of hardware design. One potential solution is to reduce the number of radio frequency (RF) chains and adopt a hybrid analog-digital precoding structure. Since the number of RF chains is much smaller than the number of antennas, the channel sampling dimension is reduced, resulting in a significant increase in pilot overhead required to accurately obtain the channel state information (CSI). Reducing pilot overhead and improving channel estimation performance in mmWave massive MIMO systems have become prominent research topics [6]. The severe path loss in the mmWave band means that only a few paths reflected by scatterers contribute to effective multipath components, leading to sparsity in the angular domain. Leveraging this angular domain sparsity, researchers have introduced a compressed sensing (CS) framework to simplify the channel estimation problem, with the goal of reducing pilot overhead and enhancing the accuracy of channel estimation [7]–[9].

Leveraging the sparsity in the angle domain, [10] employs the classic orthogonal matching pursuit (OMP) algorithm for channel recovery, where the channel is represented in the angle domain using a Fourier transform dictionary. In [11], message passing algorithm is utilized to recover the sparse angle domain channel using prior information. However, these channel estimation algorithms have the drawback of low estimation accuracy. Inspired by the powerful learning capabilities of neural networks (NN), deep learning (DL) methods have achieved remarkable results in various communication tasks such as mobility management [12], channel coding [13], CSI feedback [14], and channel estimation [15]. Among these

This article was presented in part at the IEEE International Conference on Communications, Rome, Italy, 2023 [1].

This work was supported by the Fundamental Research Funds for the Central Universities (2022JBQY004), the Natural Science Foundation of China (62221001, U2468201, W2421083), the State Scholarship Fund, China Scholarship Council (202307090109). The work of Chau Yuen was supported by the Agency for Science, Technology and Research Singapore (M22L1b0110), the Ministry of Education Singapore Tier 2 (T2EP50124-0032), the National Research Foundation (FCP-NTU-RG-2024-025). *(Corresponding authors: Bo Ai; Wei Chen.)*

Jiapan Yang, Bo Ai and Wei Chen are with the State Key Laboratory of Advanced Rail Autonomous Operation, Beijing Jiaotong University, Beijing 100044, China, and also with School of Electronic and Information Engineering, Beijing Jiaotong University, Beijing 100044, China (e-mail: {jiapanyang,boai,weich}@bjtu.edu.cn). Bo Ai is also with the School of Information Engineering, Zhengzhou University, Zhengzhou 450001, China.

Songjie Yang is with the National Key Laboratory of Wireless Communications, University of Electronic Science and Technology of China, Chengdu 611731, China. (e-mail: yangsongjie@std.uestc.edu.cn).

Ning Wang is with the School of Information Engineering, Zhengzhou University, Zhengzhou 450001, China (e-mail: ienwang@zzu.edu.cn).

Chau Yuen is with the School of Electrical and Electronics Engineering, Nanyang Technological University, Singapore 639798 (e-mail: chau.yuen@ntu.edu.sg).

works, channel estimation, as one of the key tasks, has also received extensive attention and in-depth investigation. In [16], the known values at the pilot positions are treated as a low-resolution image, and the channel is estimated using a super-resolution network cascaded with a denoising image restoration network. Three CNN-based channel estimation architectures are proposed in [17], which respectively exploit spatial-frequency correlation, temporal correlation, and pilot compression mechanisms to improve the efficiency of channel estimation. However, data-driven DL is often treated as a black-box, lacking stable performance guarantees, while reliability of communication is critically important. In contrast, the model-driven NN integrates principled algorithms with performance guarantees and DL tools, providing enhanced interpretability and reliability guarantee [18]–[20]. To improve channel estimation performance, [21] proposes a beamspace channel estimation scheme that combines Gaussian mixture distribution prior knowledge with learned approximate message passing (GM-LAMP). In [22], a channel estimator based on the learnable iterative shrinkage thresholding algorithm (LISTA) is proposed. This method is a deep unfolding of the iterative soft-thresholding algorithm, achieving lower channel estimation error. The above studies demonstrate that deep unfolding networks exhibit significant advantages in channel estimation.

With the development of 6G communication, ISAC has emerged as one of the key technologies [23]. ISAC enables simultaneous target sensing and communication by utilizing shared time and frequency resources, enhancing both spectrum and energy efficiency while improving the system's overall sensing capability [24]–[26]. Among the various ISAC design paradigms, leveraging environmental sensing to assist in communication channel estimation is particularly promising. In [27], a joint target detection and communication channel estimation method for dual-functional radar-communication (DFRC) is proposed, where radar sensing is employed to obtain target information from the environment, which is then used for communication channel path identification and parameter estimation. In [28], the authors assume that the scattering paths of the communication channel are a subset of the radar-sensed targets. By acquiring scattering angle information through radar sensing, the corresponding steer vector is used as a new sparse dictionary matrix to assist in downlink channel estimation. Since radar targets may also serve as scatterers for the communication channel, the radar and communication channels exhibit a certain degree of joint sparsity. [29] exploits this joint sparsity by utilizing the Turbo sparse Bayesian inference algorithm to achieve joint target detection and channel estimation. To reduce the pilot overhead in channel estimation, [30] leverages the echo signals received by the base station (BS) to determine the sparse basis and employs a CS algorithm to recover the channel based on user feedback. However, the target angle estimation algorithms in the aforementioned studies rely on the multiple signal classification (MUSIC) algorithm, which is limited by its high computational complexity.

The accuracy of sensing information acquisition directly impacts the overall performance of sensing-assisted communication. Existing methods for obtaining target angles can be broadly categorized into traditional methods and DL-based methods. Traditional angle estimation methods include MUSIC [31], estimation of signal parameters via rotational invariance techniques (ESPRIT) [32], and CS-based methods [33]. The MUSIC algorithm is a high-resolution angle estimation method based on subspace decomposition, suitable for ideal array. The ESPRIT leverages the rotational invariance of arrays to estimate signal parameters. CS-based methods exploit the sparsity of the angle domain to construct dictionaries and solve sparse optimization problems to estimate target angles. In recent years, DL-based DOA estimation methods have attracted widespread attention [34]–[36]. These methods leverage end-to-end NNs to automatically learn the nonlinear mapping from the covariance matrix of the received signals to the direction information, demonstrating superior estimation accuracy in complex environments. However, the aforementioned methods generally assume an ideal radar array, ignoring practical hardware imperfections such as mutual coupling, gain mismatches, and phase offsets. In practical applications, such hardware impairments can lead to considerable degradation in DOA estimation performance.

To address these challenges, researchers have proposed a series of DOA estimation methods tailored to imperfect arrays to enhance estimation accuracy [37]–[40]. A sparse Bayesian array calibration method in [38] enables high-precision DOA estimation and self-calibration under various array imperfections by employing a unified perturbation modeling framework. Leveraging DL techniques, [39] introduces a deep neural network (DNN)-based approach that denoises the covariance matrix of received signals and utilizes multiple parallel subnetworks to estimate the DOAs of multiple sources. In addition, [40] presents a CNN-based method tailored to imperfect arrays, where an innovative spatial spectrum loss function enhances estimation accuracy. Although these methods consider the situation of imperfect radar arrays, the network training process requires a large amount of data, and obtaining real data is challenging. Furthermore, the pre-trained model needs to be retrained when facing new imperfect situations, which significantly increases the computational cost in practical applications.

In this paper, we investigate channel estimation for the mmWave MIMO in V2X integrated sensing and communication scenarios. In radar-based DOA estimation, imperfect arrays can lead to significant performance degradation. Although DL-based techniques provide an efficient solution, a key limitation is that when encountering new imperfect array conditions, the network usually needs to be retrained. This introduces issues such as insufficient training data and high training resource consumption. To address this challenge, we propose a meta-learning-based DOA estimation approach for imperfect radar arrays. Subsequently, we use the angle obtained from the radar module as prior knowledge for channel estimation in the communication module. By combining this prior information with the LISTA for group row-sparsity (LISTA-GS) network, we design a new soft-threshold shrinkage function and propose the Radar-CEnet network to achieve more accurate channel estimation. The primary contributions of this paper can be summarized as follows.

- For radar sensing-based target angle estimation, we take into account the imperfections in the radar array, such as mutual coupling between antennas, positioning errors, gain inconsistencies, and nonlinear effects in the analog-to-digital converter (ADC). While these issues are often overlooked in traditional methods, they can substantially degrade the accuracy of DOA estimation in practical applications. Given the limited data available from imperfect arrays and the need to retrain existing DL networks when faced with new imperfections, we propose a novel meta-learning based DOA estimation approach for imperfect arrays. The model-agnostic meta-learning with a CNN (MAML-CNN) leverages knowledge from multiple tasks to enable the network to identify a globally optimal parameter vector. This parameter vector is used as a universal starting point, allowing the network to quickly adapt to new scenarios involving array imperfections.
- By using the radar sensing-based target angle information as prior knowledge for channel estimation, we design a deep unfolding-based radar prior-assisted sparse channel estimation network, namely Radar-CEnet. Specifically, using the angle prior information, we can identify the positions of certain non-zero elements in the sparse channel. Therefore, we design a new soft thresholding shrinkage function and propose the deep unfolding-based Radar-CEnet algorithm. The new soft thresholding function preserves the values at the positions of the non-zero elements, while shrinking the values at other positions. This enables Radar-CEnet to achieve more accurate channel estimation. Specifically, at an SNR of 20dB, the proposed Radar-CEnet method achieves approximately a 54% improvement in estimation accuracy, reducing the NMSE from –23.75dB to –27.15dB compared to the LISTA-GS method.
- We conduct a rigorous theoretical analysis of the proposed Radar-CEnet to reveal why it achieves high accurate estimation performance. The analysis shows that Radar-CEnet can leverage partially known support information as prior knowledge, leading to lower recovery errors. Additionally, the theoretical analysis proves that Radar-CEnet exhibits good convergence, providing a solid theoretical foundation for its superior performance.

The structure of this paper is as follows: Section II provides a comprehensive introduction to the system model, including the signal and channel models for communication, as well as the signal model for radar. Section III introduces the meta-learning-based angle estimation method and the proposed Radar-CEnet channel estimation method. Section IV presents the convergence analysis of the Radar-CEnet algorithm. Section V illustrates the simulation results for the meta-learning-based DOA estimation with imperfect arrays and the Radar-CEnet channel estimation. Finally, Section VI provides the conclusion of the paper.

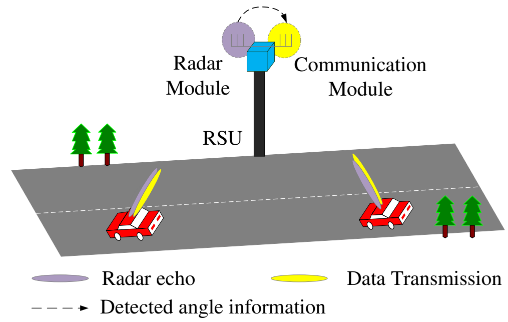

Fig. 1. An illustration of the MIMO Radar aided mmWave communication system.

Notations: Bold uppercase and lowercase letters denote matrices and vectors, respectively. For a matrix $\mathbf{A}$, $\mathbf{A}(i,:)$ and $\mathbf{A}(:,j)$ represent its i-th row and j-th column. Given index sets $\mathcal{I} \subseteq \{1,\ldots,N\}$ and $\mathcal{J} \subseteq \{1,\ldots,M\}$, $\mathbf{A}[\mathcal{I},\mathcal{J}]$ denotes the corresponding submatrix. $(\cdot)^T$ and $(\cdot)^{-1}$ denote the transpose and inverse operations, respectively. $\mathbb{R}$ and $\mathbb{C}$ represent the sets of real and complex numbers. For a vector $\mathbf{v}$, $\|\mathbf{v}\|_0$, $\|\mathbf{v}\|_1$, and $\|\mathbf{v}\|_2$ denote the ℓ_0, ℓ_1, and ℓ_2 norms, respectively, and $\mathrm{supp}(\mathbf{v})$ denotes its support. For a matrix $\mathbf{A}$, $\|\mathbf{A}\|_F$ is the Frobenius norm, while $\|\mathbf{A}\|_{2,0}$ and $\|\mathbf{A}\|_{2,1}$ denote the mixed ℓ_0/ℓ_2 and ℓ_1/ℓ_2 norms.

II. System Model

In this section, we present a radar-aided mmWave MIMO communication system. As illustrated in Fig. 1, the system is deployed in a V2X scenario, where high-speed moving vehicles serve as the user equipment (UE). The Road Side Unit (RSU) is equipped with a uniform linear array (ULA) to support simultaneous communication with M UEs. The antenna array is divided into two modules: one for communication and the other for radar. We assume that the far-field condition holds between the UEs and the antenna array.

A. Signal and Channel Model for the Communication Module

For the uplink communication, we assume that the RSU is equipped with N_{BS} antennas and N_{RF} RF chains in the communication module. The RSU communicates with M UEs, each equipped with a single antenna. The uplink channel estimation process consists of Q OFDM symbols, and each UE transmits orthogonal pilot signals to the RSU. The received baseband signal vector $\tilde{\mathbf{y}}[k,q] \in \mathbb{C}^{N_{RF}\times 1}$ for the k-th subcarrier at the q-th time slot is denoted as

$$\tilde{\mathbf{y}}[k,q] = \tilde{\mathbf{W}}[q]\tilde{\mathbf{h}}[k,q]x[k,q] + \tilde{\mathbf{n}}[k,q], \tag{1}$$

where $1 \leq k \leq K$, $1 \leq q \leq Q$. $\tilde{\mathbf{W}}[q] \in \mathbb{C}^{N_{RF}\times N_{BS}}$ represents the combining matrix that satisfies the constant modulus constraint. Specifically, $\tilde{\mathbf{W}}[q]$ can be expressed as $[\tilde{\mathbf{W}}[q]]_{m,n} = \frac{1}{\sqrt{N_{BS}}} e^{j[\boldsymbol{\Xi}]_{m,n}}$ for $1 \leq m \leq N_{BS}$, $1 \leq n \leq N_{RF}$, and $[\boldsymbol{\Xi}]_{m,n}$ is the phase value connecting the m-th antenna and the n-th RF chain. $\tilde{\mathbf{h}}[k,q] \in \mathbb{C}^{N_{BS}\times 1}$ denotes the channel vector of the k-th subcarrier and the q-th time slot. $\tilde{\mathbf{n}}[k,q] \in \mathbb{C}^{N_{RF}\times 1}$ denotes the Gaussian noise vector obeying $\mathcal{CN}(0, \sigma_n^2 \mathbf{I}_{N_{RF}})$. We assume that the pilot symbol $x[k,q]$ is 1.

Under the assumption that the channel remains static within a short time interval, by collecting Q pilot signals, the received channel matrix $\tilde{\mathbf{y}}[k]$ can be expressed as:

$$\tilde{\mathbf{y}}[k] = \tilde{\mathbf{W}}\tilde{\mathbf{h}}[k] + \tilde{\mathbf{n}}[k], \tag{2}$$

where $\tilde{\mathbf{y}}[k] = [\tilde{\mathbf{y}}^T[k,1], \cdots, \tilde{\mathbf{y}}^T[k,Q]]^T \in \mathbb{C}^{QN_{RF}}$, $\tilde{\mathbf{W}} = [\tilde{\mathbf{W}}^T[1], \cdots, \tilde{\mathbf{W}}^T[Q]]^T \in \mathbb{C}^{QN_{RF}\times N_{BS}}$, and $\tilde{\mathbf{n}}[k] = [\tilde{\mathbf{n}}^T[k,1], \cdots, \tilde{\mathbf{n}}^T[k,Q]]^T \in \mathbb{C}^{QN_{RF}}$. Then, by vertically concatenating the received vectors $\tilde{\mathbf{y}}[k]$ across K subcarriers, the composite received signal can be formulated as:

$$\tilde{\mathbf{Y}} = \tilde{\mathbf{W}}\tilde{\mathbf{H}} + \tilde{\mathbf{N}}, \tag{3}$$

where $\tilde{\mathbf{Y}} = [\mathbf{y}[1], \cdots, \tilde{\mathbf{y}}[K]] \in \mathbb{C}^{QN_{RF}\times K}$, $\tilde{\mathbf{H}} \in \mathbb{C}^{N_{BS}\times K}$ denotes the channel matrix, and $\tilde{\mathbf{N}} = [\tilde{\mathbf{n}}[1], \cdots, \tilde{\mathbf{n}}[Q]] \in \mathbb{C}^{QN_{RF}\times K}$.

The geometric channel model is employed to characterize the channel in the mmWave massive MIMO V2X communication system. The mmWave channel for the k-th subcarrier and the q-th time slot is given by

$$\tilde{\mathbf{h}}[k,q] = \sqrt{\frac{N_{BS}}{L}} \sum_{l=1}^{L} \alpha_{l,q} e^{-j2\pi(f_s \tau_l \frac{k}{K} - f_l q)} \mathbf{a}(\phi_l), \tag{4}$$

where $\alpha_{l,q}$ is the complex gain of the l-th path, which follows a distribution of $\mathcal{CN}(0, \sigma^2)$. The system sampling rate is denoted by f_s, while f_l corresponds to the Doppler frequency shift of the l-th path, ϕ_l indicates the angle of arrival (AOA) of the l-th path at the RSU, and τ_l represents the delay associated with the l-th path. Given that the RSU is equipped with a ULA, the array steering vector $\mathbf{a}(\phi) \in \mathbb{C}^{N_{BS}\times 1}$ can be defined as

$$\mathbf{a}(\phi) = \frac{1}{\sqrt{N_{BS}}}[1, e^{-j\frac{2\pi d}{\lambda}\sin(\phi)}, \cdots, e^{-j\frac{2\pi d}{\lambda}(N_{BS}-1)\sin(\phi)}]^T, \tag{5}$$

where d is the antenna spacing satisfying $d = \lambda/2$, and λ is the carrier wavelength.

B. Signal Model for the Radar Module

The radar module is based on a monostatic radar configuration, where the number of array elements for transmission and reception is the same, denoted as Z. The transmitted signal vector for all Z elements can be expressed as

$$\mathbf{r}(n) = [r_1(n), r_2(n), \cdots, r_Z(n)]^T, n = 1, 2, \cdots, N, \tag{6}$$

where N is the total number of snapshots. We assume that the transmitted signals are orthogonal to each other, resulting in no correlation between different signals. The corresponding correlation matrix can be simplified to the identity matrix $\mathbf{I}_Z$, indicating that the energy is evenly distributed in the spatial domain.

For M target UEs, the echo signal received by Z antennas is given by

$$\mathbf{y}_r(n) = \sum_{m=1}^{M} \beta_m \mathbf{b}_r(\theta_m)\mathbf{b}_t^*(\theta_m)\mathbf{r}(n) + \mathbf{w}(n), \tag{7}$$

where $\mathbf{y}_r(n) = [y_1(n), y_2(n), \cdots, y_Z(n)]^T$ represents the received echo signal vector. The reflection coefficient of the m-th UE is denoted as $\beta_m \sim \mathcal{CN}(0, \sigma_{\beta_m}^2)$, while the noise is represented by $\mathbf{w}(n) \sim \mathcal{CN}(0, \sigma_w^2 \mathbf{I}_Z)$. Moreover, $\mathbf{b}_t(\theta_m)$ and $\mathbf{b}_r(\theta_m)$ represent the steering vectors for the transmitting and receiving antennas, respectively. The expressions for $\mathbf{b}_r(\theta_m)$ and $\mathbf{b}_t(\theta_m)$ are similar, and $\mathbf{b}_t(\theta_m)$ satisfies

$$\mathbf{b}_t(\theta_m) = \frac{1}{\sqrt{Z}}[1, e^{j\frac{2\pi d}{\lambda}\sin(\theta_m)}, \cdots, e^{j\frac{2\pi d}{\lambda}(Z-1)\sin(\theta_m)}]^T, \tag{8}$$

where d is the distance between adjacent antenna elements, λ denotes the propagation signal wavelength, and θ_m denotes the azimuth angle of the m-th UE. We assume that θ_m of the UE are distinct and randomly distributed within the range $(-\frac{\pi}{2}, \frac{\pi}{2})$.

In the radar received signal, the following types of array imperfections are considered.

1) The Mutual Coupling Effect: Since antennas cannot achieve perfect isolation, when the spacing between antenna elements is small or the carrier frequency is high, the interaction of the spatial EM field leads to EM coupling effects. Due to the MIMO characteristics of the radar, the mutual coupling effects between array elements become significant and cannot be ignored. We use the complex matrices $\mathbf{C}_t$ and $\mathbf{C}_r$ to represent the mutual coupling effects of the transmitting and receiving antennas, respectively. Since $\mathbf{C}_t$ and $\mathbf{C}_r$ are generated in the same way, we only describe the generation method of $\mathbf{C}_t$ here. The diagonal elements of $\mathbf{C}_t$ are set to 1. The mutual coupling coefficient between the zth and z'th $(z \neq z')$ antenna is $\mathbf{C}_{t,z,z'} \in \mathbb{C}$ with $|\mathbf{C}_{t,z,z'}| < 1$. The entry at the zth row and the z'th column is denoted as

$$\mathbf{C}_{t,z,z'} = |\mathbf{C}_{t,z,z'}|e^{j\psi_{z,z'}}, \tag{9}$$

and $\mathbf{C}_{t,z,z'}$ is determined by a uniform distribution $|\mathbf{C}_{t,z,z'}| \in [0, \sigma_{mc}]$ with $z \neq z'$. The phase $\psi_{z,z'}$ follows a uniform distribution $\psi_{z,z'} \in [0, 2\pi]$. The steering vector considering the mutual coupling effects is expressed as:

$$\begin{aligned} \tilde{\mathbf{b}}_t(\theta_m) &= \mathbf{C}_t \mathbf{b}_t(\theta_m), \\ \tilde{\mathbf{b}}_r(\theta_m) &= \mathbf{C}_r \mathbf{b}_r(\theta_m). \end{aligned} \tag{10}$$

2) The Position Perturbation: The actual antenna positions may deviate from their intended locations, leading to phase errors in the received signals among antennas within the steering vector. The position perturbation follows a Gaussian distribution with the mean of 0, while the standard deviation σ_{per} is chosen from a uniform distribution $\sigma_{per} \in [0, \sigma_{max\_per}]$.
3) Gain and Phase Errors: The RF channels typically cannot achieve completely consistent performance, resulting in amplitude and phase errors in the received signals. Since $\tilde{\mathbf{b}}_t(\theta_m)$ and $\tilde{\mathbf{b}}_r(\theta_m)$ are generated in the same way, we only describe the generation method of $\tilde{\mathbf{b}}_t(\theta_m)$.

The array response considering gain and phase errors $\Delta\mathbf{b}_t$ and $\Delta\theta_m$ is expressed as follows.

$$\tilde{\mathbf{b}}_t(\theta_m) = (|\mathbf{b}_t| + |\Delta\mathbf{b}_t|)\exp\{j(\theta_m + \Delta\theta_m)\}. \tag{11}$$

The interference among elements is random and mutually independent. The generation of $\Delta\mathbf{b}_t$ and $\Delta\theta_m$ are as follows:

$$\begin{aligned} &\Delta\mathbf{b}_t \sim \mathcal{N}(0, \sigma^2_{\text{gain}}), \quad \sigma_{\text{gain}} \in [0, \sigma_{\text{max\_gain}}], \\ &\Delta\theta_m \sim \mathcal{N}(0, \sigma^2_{\text{phase}}), \quad \sigma_{\text{phase}} \in [0, \sigma_{\text{max\_phase}}]. \end{aligned} \tag{12}$$

4) The Nonlinear Effect: The RF chains and analog-to-digital converters (ADCs) introduce additional nonlinear effects. We model the nonlinear operation in the receiving channels using a nonlinear function $g(\cdot)$, which is expressed as

$$g(x) = \tanh(x\sigma_{nonlinear}), \tag{13}$$

where $\sigma_{nonlinear}$ is an adjustable parameter used to influence the amplitude of the nonlinear activation function.

Considering the case of an imperfect array, the received signal model is rewritten as:

$$\tilde{\mathbf{y}}_r(n) = g\Big(\sum_{m=1}^{M} \beta_m \tilde{\mathbf{b}}_r(\theta_m)\tilde{\mathbf{b}}_t^*(\theta_m)\mathbf{r}(n)\Big) + \mathbf{w}(n). \tag{14}$$

The received signal covariance matrix can be calculated as

$$\mathbf{R}_{y_r} = \frac{1}{N}\sum_{n=1}^{N} \tilde{\mathbf{y}}_r(n)\tilde{\mathbf{y}}_r^H(n). \tag{15}$$

The direction of arrival (DOA) estimation problem can be modeled as a parameter estimation problem based on the covariance matrix $\mathbf{R}_{y_r}$.

III. The Proposed method for Channel Estimation

In this section, we present the uplink transmission frame structure for the MIMO radar aided mmWave communication system. As illustrated in Fig. 2, the duration of each frame is denoted as T_e, which consists of several slots. The duration of a single pilot is represented by T_s, while P_1 and P_2 refer to the number of pilots employed by the radar for angle training and tracking, respectively. In the radar module, AoA training and AoA tracking are represented by P_1T_s and P_2T_s, respectively. The AoA training refers to the total time required for the AoA estimation algorithm in the radar system. In the communication module, multiple time slots are allocated. Additionally, each time slot is made up of path gain training and data transmission, corresponding to the C_G and C_D pilots, respectively.

Assuming that the UE is affected by the large-scale characteristics of the scattering environment, the channel varies relatively slowly and remains essentially stable within a certain period of time. Meanwhile, the RSU antenna is typically positioned at a much higher altitude compared to the moving vehicles. Therefore, it is clear that the transmission between

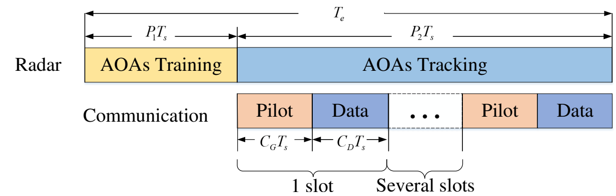

Fig. 2. The transmission frame structure for the MIMO Radar and communication system.

the UEs and the RSU is primarily governed by the line-of-sight (LoS) path. During communication between the moving vehicles and the RSU, the radar rapidly detects the direction of the targets and transmits the detection results to the communication module. As a result, the angle information provided by the MIMO radar is utilized to assist in the channel estimation of the communication module.

A. Meta-Learning Based Angles Estimation

Currently, most existing DL-based DOA estimation methods for imperfect radar arrays are designed for specific types of array imperfections. When new forms of imperfections occur, these methods usually require collecting large amounts of new data and retraining the network. This process faces two main challenges: first, constructing datasets for new array imperfections is highly difficult; second, retraining the DL network often consumes considerable time and computational resources. To address these issues, we propose leveraging meta-learning techniques to solve the DOA estimation problem in imperfect arrays. The core idea of meta-learning is to learn shared patterns from multiple tasks and use these patterns to help the model learn more efficiently when faced with unseen tasks. Model-agnostic meta-learning (MAML) is a classic meta-learning method. It works by finding a good initial model that can be quickly fine-tuned across multiple tasks, enabling fast adaptation to new tasks. We combine MAML with a CNN network, and by training on multiple DOA estimation tasks with different imperfect arrays, the network learns to find a good set of initial parameters. This allows the network to rapidly adapt to new DOA estimation tasks for imperfect arrays with only a small amount of data.

The MAML-CNN algorithm relies on data from multiple imperfect array conditions for training. Therefore, we formulate the DOA estimation problems of different imperfect array conditions as separate tasks. Let the task set be denoted as $\{\mathcal{T}_{\tilde{m}}, \tilde{m} = 1, 2, \ldots, \tilde{M}\}$, consisting of $\tilde{M}$ tasks. For each task $\mathcal{T}_{\tilde{m}}$, we establish the received signal-DOA pairs and construct a training dataset $\mathbb{S}_{\tilde{m}}$ and a testing dataset $\mathbb{Q}_{\tilde{m}}$.

Meanwhile, we introduce the CNN structure. The primary function of the CNN network is to learn the mapping from the covariance matrix $\mathbf{R}_{\mathbf{y_r}}$ to the target angles θ_{radar}, which can be expressed as:

$$\theta_{radar} = F(\mathbf{R}_{\mathbf{y_r}}, \varphi_{radar}), \tag{16}$$

where $F(\cdot)$ represents the mapping function parameterized by the CNN parameters φ_{radar}. The structure of the CNN consists of 3 two-dimensional convolutional layers, 3 batch

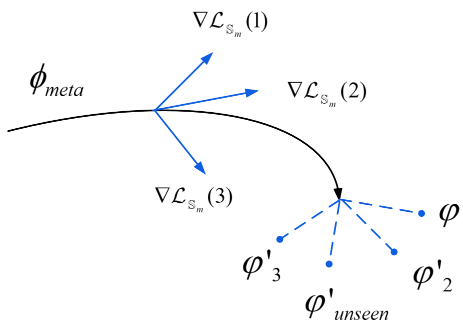

Fig. 3. The diagram of the meta-learning algorithm that can optimize the model parameter for quickly adapting to the unseen unperfect array.

normalization layers, 3 pooling layers, and 3 linear layers. Specifically, each convolutional layer employs 3×3 convolutional kernels. The first convolutional layer consists of 32 filters, the second layer contains 64 filters, and the third layer comprises 128 filters. Each convolutional layer is followed by a batch normalization layer, a ReLU activation function, and a max pooling layer with a stride of 2 and a pooling window size of 2×2. The final output of the CNN architecture is the estimated DOA.

To better introduce meta-learning method, We first introduce the learning strategy for a single task. For example, when training a CNN for task $\mathcal{T}_{\tilde{m}}$, the trainable parameters are typically initialized randomly. Then, the training dataset $\mathbb{S}_{\tilde{m}}$ is used to iteratively update the parameters using stochastic gradient descent (SGD)

$$\boldsymbol{\varphi}_{\tilde{m}} = \boldsymbol{\varphi} - \alpha \nabla_{\boldsymbol{\varphi}} \mathcal{L}_{\mathbb{S}_{\tilde{m}}}(\boldsymbol{\varphi}), \tag{17}$$

where $\boldsymbol{\varphi}$ represents the randomly initialized parameter vector, and $\boldsymbol{\varphi}_{\tilde{m}}$ represents the optimized network parameter vector for task $\mathcal{T}_{\tilde{m}}$. The learning rate is represented by α, and $\nabla_{\boldsymbol{\varphi}}$ denotes the gradient with respect to $\boldsymbol{\varphi}$. The loss function $\mathcal{L}_{\mathbb{S}_{\tilde{m}}}$ represents the mean square error (MSE) evaluated on the dataset $\mathbb{S}_{\tilde{m}}$.

In contrast to the traditional learning strategy, meta-learning seeks to determine a parameter vector $\boldsymbol{\phi}_{meta}$ by leveraging knowledge from multiple tasks. Specifically, the optimization objective of meta-learning is formulated as

$$\begin{aligned}\boldsymbol{\phi}_{meta} &= \arg\min_{\boldsymbol{\phi}} \sum_{\tilde{m}=1}^{\tilde{M}} \mathcal{L}_{\mathbb{Q}_{\tilde{m}}}(\boldsymbol{\varphi}_{\tilde{m}}^{'}) \\ &= \arg\min_{\boldsymbol{\phi}} \sum_{\tilde{m}=1}^{\tilde{M}} \mathcal{L}_{\mathbb{Q}_{\tilde{m}}}(\boldsymbol{\phi} - \alpha \nabla_{\boldsymbol{\phi}} \mathcal{L}_{\mathbb{S}_{\tilde{m}}}(\boldsymbol{\phi})),\end{aligned} \tag{18}$$

where $\boldsymbol{\varphi}_{\tilde{m}}^{'}$ is the task-specific parameter vector and $\boldsymbol{\phi}$ is the initial parameter vector. To better explain the basic principle of the meta-learning, the diagram of the meta-learning algorithm is illustrated in Fig. 3. Next, we introduce our proposed MAML-CNN method for DOA estimation with imperfect arrays. As shown in Fig. 4, MAML-CNN consists of two stages: meta-training and meta-testing.

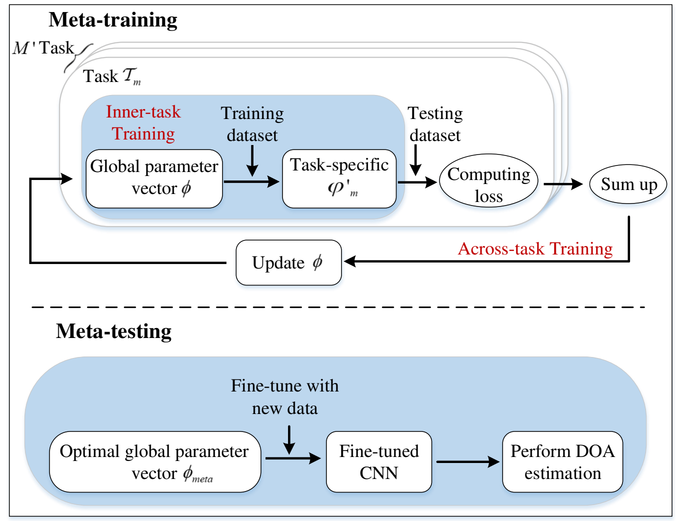

Fig. 4. The proposed MAML-CNN method for DOA estimation under imperfect array.

1) Meta-training: The meta-training includes both inner-task training and across-task training. The global parameter vector is updated once after each meta-training iteration.

During the i-th iteration of meta-training, with $i = 1, 2, \ldots, I$ and I being the total number of iterations. We randomly select $\tilde{M}'$ tasks from the total $\tilde{M}$ tasks for inner-task training. In the i-th meta-training iteration, the global parameter to be optimized is $\boldsymbol{\phi}_{i-1}$. For each of the $\tilde{M}'$ task, we can compute a temporary task-specific parameter vector $\boldsymbol{\varphi}'_{\tilde{m}}$ based on $\boldsymbol{\phi}_{i-1}$. Specifically, $\boldsymbol{\varphi}'_{\tilde{m}}$ is obtained by minimizing the cost of the loss function over the training dataset $\mathbb{S}_{\tilde{m}}$ for task $\mathcal{T}_{\tilde{m}}$. The inner-task training process can be given by

$$\boldsymbol{\varphi}'_{\tilde{m}} = \boldsymbol{\phi}_{i-1} - \alpha \nabla_{\boldsymbol{\phi}_{i-1}} \mathcal{L}_{\mathbb{S}_{\tilde{m}}}(\boldsymbol{\phi}_{i-1}). \tag{19}$$

After finishing $\tilde{M}'$ rounds of inner-task training, we can obtain $\{\boldsymbol{\varphi}'_1, \boldsymbol{\varphi}'_2, \ldots, \boldsymbol{\varphi}'_{\tilde{M}'}\}$, which will be used for across-task training.

The goal of the across-task training is to improve the network's adaptability to multiple tasks by optimizing the global parameter vector $\boldsymbol{\phi}_{i-1}$. Specifically, the network's performance with the initial parameter $\boldsymbol{\phi}_{i-1}$ can be assessed by computing its MSE loss on the testing dataset of each task, thereby evaluating its adaptability. By minimizing the total MSE loss across the testing datasets of $\tilde{M}'$ tasks, the optimized global parameter vector $\boldsymbol{\phi}_i$ can be obtained

$$\boldsymbol{\phi}_i = \boldsymbol{\phi}_{i-1} - \beta \nabla_{\boldsymbol{\varphi}'_{\tilde{m}}} \sum_{\tilde{m}=1}^{\tilde{M}'} \mathcal{L}_{\mathbb{Q}_{\tilde{m}}}(\boldsymbol{\varphi}'_{\tilde{m}}), \tag{20}$$

where β is the across-task learning rate.

The distinction between inner-task training and across-task training lies in their focus: inner-task training is performed independently for each specific task, with an emphasis on optimizing task-related parameters to enhance the model's performance on that task. In contrast, across-task training uses the results from inner-task training to further refine the global

Algorithm 1 MAML-CNN DOA Estimation Algorithm

Input: Training task set $\{\mathcal{T}_1, \mathcal{T}_2, \ldots, \mathcal{T}_{\tilde{M}}\}$, where each task $\tilde{m}$ is associated with a training dataset $\{\mathbb{S}_{\tilde{m}}\}$ and a testing dataset $\{\mathbb{Q}_{\tilde{m}}\}$;

Output: Optimized global parameter vector $\boldsymbol{\phi}_{meta}$ and the fine-tuned CNN;

```
Randomly initialize φ;
Meta-training
For l = 1, 2, ..., L do
    Sample M̃' tasks from {T_1, T_2, ..., T_M̃};
    for all M̃' tasks do
        Update task-specific parameters using (19);
    end for;
    Update the globel parameter using (20);
end for
Return φ_meta = φ_L
Meta-testing
Fine-tune the CNN with φ_meta and estimate the DOA.
```

parameter vector, thereby improving the model's generalization ability. By alternately applying inner-task training and across-task training, the global parameters are progressively refined, ultimately resulting in the optimal global parameter $\boldsymbol{\phi}_{meta} = \boldsymbol{\phi}_I$.

2) Meta-testing: Meta-testing refers to the ability of the network to quickly adapt and perform DOA estimation in the case of imperfect arrays. Unlike traditional learning strategies that require training from scratch, it only requires fine-tuning based on the global parameter vector $\boldsymbol{\phi}_{meta}$. Since $\boldsymbol{\phi}_{meta}$ encompassses general knowledge applicable to a wide range of imperfect array, the CNN can quickly converge to the optimal state with just a few gradient descent updates, enabling efficient and accurate DOA estimation.

The steps for the proposed MAML-CNN DOA estimation method are summarized in Algorithm 1.

B. The Proposed Radar-CEnet Channel Estimation Method

Massive MIMO channels exhibit sparsity in the angle domain. To represent this sparse model, we construct a redundant dictionary $\tilde{\mathbf{D}}$ that transform the spatial-frequency domain channel $\tilde{\mathbf{H}}$ into the angle-frequency domain channel $\tilde{\mathbf{H}}^a \in \mathbb{C}^{G\times K}$, which is given by

$$\tilde{\mathbf{H}} = \tilde{\mathbf{D}}\tilde{\mathbf{H}}^a, \tag{21}$$

where $\tilde{\mathbf{D}} = [\mathbf{a}(\phi_1), \mathbf{a}(\phi_2), \cdots, \mathbf{a}(\phi_G)] \in \mathbb{C}^{N_{BS}\times G}$ represents the redundant dictionary matrix, where G corresponds to the number of grids. $\mathbf{a}(\phi_g)$ represents the corresponding array steering vector in (5). The sets of the quantized virtual angles can be written as

$$\mathit{\Gamma}_R = \{\phi_g : \sin(\phi_g) = -1 + 2(g-1)/G, g = 1, \ldots, G+1\}. \tag{22}$$

Therefore, the received signal expression (3) can be rewritten as

$$\tilde{\mathbf{Y}} = \tilde{\mathbf{W}}\tilde{\mathbf{D}}\tilde{\mathbf{H}}^a + \tilde{\mathbf{N}} = \tilde{\mathbf{A}}\tilde{\mathbf{H}}^a + \tilde{\mathbf{N}}, \tag{23}$$

where $\tilde{\mathbf{H}}^a \in \mathbb{C}^{G\times K}$, and $\tilde{\mathbf{A}} = \tilde{\mathbf{W}}\tilde{\mathbf{D}} \in \mathbb{C}^{QN_{RF}\times G}$ represents the effective measurement matrix. Notably, $\tilde{\mathbf{H}}^a$ demonstrates group row-sparsity. To facilitate algorithm design, we transform the complex matrix into a real-valued matrix by separating its real and imaginary parts. After the transformation, the real-valued received signal can be expressed as:

$$\mathbf{Y} = \mathbf{A}\mathbf{H}^a + \mathbf{N}, \tag{24}$$

where $\mathbf{Y} \in \mathbb{R}^{2QN_{RF}\times K}, \mathbf{H} \in \mathbb{R}^{2G\times K}, \mathbf{N} \in \mathbb{R}^{2QN_{RF}\times K}$ represent the real-valued forms of the complex matrices $\tilde{\mathbf{Y}}, \tilde{\mathbf{H}}^a, \tilde{\mathbf{N}}$, constructed by stacking their real and imaginary parts. For the complex sensing matrix $\tilde{\mathbf{A}}$, its equivalent real-valued matrix $\mathbf{A} \in \mathbb{R}^{2QN_{RF}\times 2G}$ is defined as:

$$\mathbf{A} = \begin{bmatrix} Re\{\tilde{\mathbf{A}}\} & -Im\{\tilde{\mathbf{A}}\} \\ Im\{\tilde{\mathbf{A}}\} & Re\{\tilde{\mathbf{A}}\} \end{bmatrix}, \tag{25}$$

where $Re\{\cdot\}$ and $Im\{\cdot\}$ represent the real part and imaginary part of the complex matrixs. Given the received signals, the channel matrix $\mathbf{H}^a$ can be estimated by solving the following optimization problem

$$\begin{aligned} &\min_{\mathbf{H}^a} \|\mathbf{H}^a\|_{row,0} \\ &\text{s.t. } \|\mathbf{Y} - \mathbf{A}\mathbf{H}^a\|_F \le \delta, \end{aligned} \tag{26}$$

where $\|\cdot\|_{row,0}$ denotes the number of non-zero rows of the input matrix. δ is the error tolerance parameter. The above problem is a multiple measurement vectors (MMV) sparse recovery problem [41]. It can be solved using CS algorithms, such as the simultaneous orthogonal matching pursuit (SOMP) algorithm [42] and the iterative soft thresholding algorithm for group row-sparsity (ISTA-GS). Next, we primarily introduce the ISTA-GS algorithm.

ISTA-GS introduces group sparsity regularization, applying sparsity constraints to all rows and forcing the overall norm of certain rows to be zero, thereby achieving row sparsity. In addition, ISTA-GS uses group soft thresholding, ensuring that all elements of a row are either completely removed or scaled together, further ensuring group row-sparsity. ISTA-GS estimates the channel $\mathbf{H}^a$ through iterative recursive calculations:

$$\mathbf{H}^a_{t+1} = \eta_{\theta_t}(\mathbf{H}^a_t + \frac{1}{\lambda}\mathbf{A}^T(\mathbf{Y} - \mathbf{A}\mathbf{H}^a_t)), \tag{27}$$

where $\mathbf{H}^a_t$ is the estimated channel at iteration t, λ is the maximum eigenvalue of $\mathbf{A}^T\mathbf{A}$, and θ_t is the threshold of the algorithm at the t-th iteration. The group soft-thresholding function [43] is represented by $\eta_\theta(\cdot)$. The definition of $\eta_\theta(\cdot)$:

$$\eta_\theta(\mathbf{H}^a(s,:)) = \max\left\{0, \frac{\|\mathbf{H}^a(s,:)\|_2 - \theta}{\|\mathbf{H}^a(s,:)\|_2}\right\}\mathbf{H}^a(s,:), \tag{28}$$

where $\mathbf{H}^a(s,:)$ denotes the s-th row of $\mathbf{H}^a$. However, the ISTA-GS algorithm typically requires a large number of iterations to converge, which limits its efficiency in practice. In order to tackle this problem, a learning-based ISTA-GS (LISTA-

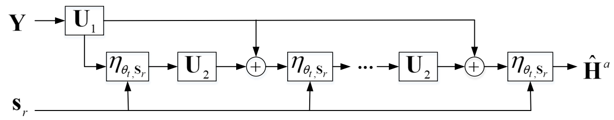

Fig. 5. The proposed Radar-CEnet algorithm for communication channel estimation.

GS) method is proposed in [43]. By denoting $\mathbf{U}_1 = \frac{1}{\lambda}\mathbf{A}^T$ and $\mathbf{U}_2 = \mathbf{I} - \frac{1}{\lambda}\mathbf{A}^T\mathbf{A}$, (27) can be rewritten as

$$\mathbf{H}^a_{t+1} = \eta_{\theta_t}(\mathbf{U}_1\mathbf{Y} + \mathbf{U}_2\mathbf{H}^a_t), \tag{29}$$

where $\mathbf{U}_1$, $\mathbf{U}_2$ and $\{\theta_t\}_1^T$ are the learnable parameters.

To enhance the channel estimation performance, we consider using the angle obtained from the radar module as prior knowledge for communication channel estimation. Inspired by the method in [44], we propose a prior-information-assisted Radar-CENet to address sparse channel estimation with partially known support. Unlike the method in [44], our approach specifically targets the recovery of sparse signals with group row-sparse structure in the context of the MMV problem.

In the Radar-CEnet network, the positions of the non-zero rows are first determined based on the angles obtained from the radar module. We use the vector $\mathbf{s}_r$ to store the known non-zero row information. The elements in the $\mathbf{s}_r$ vector have two possible values: 0 and 1. An element with a value of 1 indicates a non-zero row with prior information, while an element with a value of 0 represents a row without prior information. In the network, $\mathbf{Y}$ and $\mathbf{s}_r$ are provided as inputs, while the network outputs the estimated channel $\mathbf{H}^a$. Based on the LISTA-GS method, the t-th layer of the proposed Radar-CEnet is formulated as follows:

$$\mathbf{H}^a_{t+1} = \eta_{\theta_t,\mathbf{s}_r}(\mathbf{U}_1\mathbf{Y} + \mathbf{U}_2\mathbf{H}^a_t), \tag{30}$$

where the initial threshold θ_0 is 0.1. $\eta_{\theta_t,\mathbf{s}_r}$ is a new soft thresholding function designed based on the prior information vector $\mathbf{s}_r$, and it is defined as follows.

$$\eta_{\theta_t,\mathbf{s}_r}(\mathbf{h}[i]) = \begin{cases} \mathbf{h}[i] & \mathbf{s}_r[i] = 1 \\ \frac{\|\mathbf{h}[i]\|_2 - \theta_t}{\|\mathbf{h}[i]\|_2}\mathbf{h}[i] & \|\mathbf{h}[i]\|_2 > \theta_t, \mathbf{s}_r[i] = 0 \\ 0 & \|\mathbf{h}[i]\|_2 \le \theta_t, \mathbf{s}_r[i] = 0, \end{cases} \tag{31}$$

where $\mathbf{h}[i]$ is the i-th row of $\mathbf{H}^a$. This thresholding function preserves the values from known prior information and performs group soft thresholding for rows without prior information.

Fig. 5 illustrates the structure of the proposed Radar-CEnet. As shown in the figure, the input of Radar-CEnet are the received signal $\mathbf{Y}$ and the prior information $\mathbf{s}_r$. Since this prior information indicates the true positions of the non-zero rows of $\mathbf{H}^a$, we use this true support to assist sparse channel estimation, thereby reducing the learning difficulty of the network. Specifically, when the element value of $\mathbf{s}_r$ is 1, the original value of the row is preserved.

Algorithm 2 Training procedure for Radar-CEnet

Training Data: A batch of training data $\{\mathbf{Y}_p, \mathbf{s}_{r,p}, \mathbf{H}^a_p\}_{p=1}^P$ constructed based on equation (24)
Initialization:$\mathbf{U}_1 = \frac{1}{\lambda}\mathbf{A}^T$, $\mathbf{U}_2 = \mathbf{I} - \frac{1}{\lambda}\mathbf{A}^T\mathbf{A}$, $\{\theta_t\}_{t=1}^T = 0.1$
Goal: Optimize the parameter set $\Theta = \{\mathbf{U}_1, \mathbf{U}_2, \{\theta^t\}_{t=1}^T\}$ for Radar-CEnet
For each batch training pairs $\{\mathbf{Y}_p, \mathbf{s}_{r,p}, \mathbf{H}^a_p\}_{p=1}^P$
    calculate the gradient of Θ according to the loss
    update Θ using the ADAM optimizer
end for

The network is trained in an end-to-end manner using the MSE loss function, which is expressed as

$$\mathcal{L}(\mathbf{\Theta}) = \sum_{p=1}^P \left\| \hat{\mathbf{H}}^a_p - \mathbf{H}^a_p \right\|_F^2 = \sum_{p=1}^P \left\| \mathbf{R}(\mathbf{Y}, \mathbf{\Theta}) - \mathbf{H}^a_p \right\|_F^2, \tag{32}$$

where P represents the number of training data within each batch. $\hat{\mathbf{H}}^a$ represents the output of the Radar-CEnet. $\mathbf{R}(\cdot)$ denotes the processing of network, and $\mathbf{\Theta} = \{\mathbf{U}_1, \mathbf{U}_2, \theta_t\}_{t=0}^{T_1}$ is the set of learnable parameters. T_1 denotes the number of layers of the network. The training procedure of Radar-CEnet is given in Algorithm 2.

IV. Convergence Analysis

In this section, we present the main theoretical results of the proposed Radar-CEnet method. Since the proposed method inherits the structure of ISTA-GS, this enables us to explore the interpretability of the DL framework from an optimization perspective. However, the complexity arising from dimensional unfolding and matrix structures poses unique and significant challenges to the theoretical analysis of unfolded neural networks.

LISTA-GS is a learning-based version of the ISTA-GS method. LISTA-GS achieves better performance because the neural network can find more optimal weight parameters. Various work [44]–[46] prove that weight matrixes need to satisfy certain conditions. In this paper, the proposed Radar-CEnet is also subject to such constraints.

Theorem 1: **[Necessary Condition]** Consider a noiseless measurement

$$\mathbf{Y} = \mathbf{A}\mathbf{H}^a, \|\mathbf{H}^a\|_{row,0} \le E_s. \tag{33}$$

If the Radar-CEnet given in (30) can converge to the sparse channel $\mathbf{H}^{a*}$, then two weight matrixes $\{\mathbf{U}_1, \mathbf{U}_2\}$ of the Radar-CEnet satisfy the following structure

$$\mathbf{U}_{2,t} = \mathbf{I} - \mathbf{U}_{1,t}\mathbf{A}. \tag{34}$$

The proof of this theorem is provided in [47].

Definition 1: The t-th layer of Radar-CEnet with the signal weight matrix is defined by the following iterative of the form

$$\mathbf{H}^a_{t+1} = \eta_{\theta_t,\mathbf{s}_r}(\mathbf{H}^a_t + (\mathbf{U}_t)^T(\mathbf{Y} - \mathbf{A}\mathbf{H}^a_t)), \tag{35}$$

where $\mathbf{U}_t = (\mathbf{U}_1^t)^T$. Next, given this weight constraint, we study the convergence of the Radar-CEnet.

For theoretical analysis, we assume the matrix $\mathbf{H}^{a*}$ and noise $\mathbf{N}$ belong to the set:

$$\begin{aligned}\mathcal{H}(\beta, E_s, \sigma) = &\{(\mathbf{H}^{a*}, \mathbf{N}) | \|\mathbf{H}^{a*}[i,:]\|_2 \leq \beta, \forall i, \\ &\|\mathbf{H}^{a*}\|_{row,0} \leq E_s, \|\mathbf{N}\|_F \leq \sigma\}.\end{aligned} \quad (36)$$

In other words, $\mathbf{H}^{a*}$ and $\mathbf{N}$ are bounded, and $\mathbf{H}^{a*}$ contains no more than E_s non-zero rows.

Theorem 2: **[Convergence Rate of Radar-CEnet]** Given $\{\mathbf{U}, \theta_t\}_{t=1}^{T_1}$, let $\{\mathbf{H}_t^a\}_{t=1}^{T_1}$ be generated by Rardar-CEnet with layers in (30). The initial point is set as $\mathbf{H}_0^a = 0$. If E_s is sufficiently small, then $(\mathbf{H}^{a*}, \mathbf{Z}) \in \mathcal{H}(\beta, E_s, \sigma)$, and the error bound is given by:

$$\sup_{(\mathbf{H}^{a*}, \mathbf{N})} \|\mathbf{H}_{t+1}^a - \mathbf{H}^{a*}\|_F \leq E_s \beta exp(-\alpha t) + A\sigma, \quad (37)$$

where $\alpha > 0$ and $A > 0$ are positive constants. For the noiseless case, i.e., $\sigma = 0$, it can be observed that as the number of layers approaches infinity, the error bound decreases to 0 at a linear rate.

To prove Theorem 2, we proceed with three steps: First, we define the optimal parameters that guarantee the algorithm's convergence. Second, we establish an error bound for an individual sample. Finally, we obtain an error bound for the complete sample set.

A. Optimal Parameters for Learning

In this subsection, we define the optimal learned parameters in the Radar-CEnet algorithm that ensure a linear convergence rate.

First, let's introduce some essential definitions, beginning with the concept of mutual coherence.

Definition 2: The mutual coherence μ of $\mathbf{A} \in \mathbb{R}^{Q2N_{RF} \times 2G}$ can be described as

$$\mu(\mathbf{A}) = \max_{\substack{i \neq j \\ 1 \leq i,j \leq 2G}} |\mathbf{A}[:,i]^T \mathbf{A}[:,j]|. \quad (38)$$

The definition of the generalized mutual coherence of $\mathbf{A}$, with its columns normalized, is given by

$$\widetilde{\mu}(\mathbf{A}) = \inf_{\substack{\mathbf{U} \in \mathbb{R}^{2QN_{RF} \times 2G} \\ (\mathbf{U}[:,i])^T \mathbf{A}[:,i] = 1}} \left\{ \max_{\substack{i \neq j \\ 1 \leq i,j \leq 2G}} |\mathbf{U}[:,i]^T \mathbf{A}[:,j]| \right\}. \quad (39)$$

The primary difference between $\mu(\mathbf{A})$ and $\widetilde{\mu}(\mathbf{A})$: $\mu(\mathbf{A})$ directly measures the maximum correlation between columns of the original matrix $\mathbf{A}$, and serves as a static metric. $\widetilde{\mu}(\mathbf{A})$ introduces a transformation matrix $\mathbf{U}$, dynamically optimizing the lower bound of correlation and providing a more robust measure. In general, $\widetilde{\mu}(\mathbf{A}) \leq \mu(\mathbf{A})$, since the generalized mutual coherence considers the optimal case over all possible transformations.

Lemma 1: There exists a matrix $\mathbf{U} \in \mathbb{R}^{2QN_{RF} \times 2G}$ satisfying the infimum given in (39) and the set of optimal weight matrices is defined as

$$\begin{aligned}\mathcal{U}(\mathbf{A}) = \arg\min_{\mathbf{U} \in \mathbb{R}^{2QN_{RF} \times 2G}} \Big\{ &(\mathbf{U}[:,i])^T \mathbf{A}[:,i] = 1, \forall i, \\ &\max_{\substack{i \neq j \\ 1 \leq i,j \leq 2G}} |\mathbf{U}[:,i]^T \mathbf{A}[:,j]| = \widetilde{\mu}(\mathbf{A}) \Big\}.\end{aligned} \quad (40)$$

The proof of this lemma follows the process outlined in [46].

Next, we define the optimal parameters that Radar-CEnet aims to learn as follows.

Definition 3: $\mathbf{\Theta} = \{\mathbf{U}_t, \theta_t\}_{t=0}^{\infty}$ are optimal parameters in Radar-CEnet if they satisfy

$$\begin{aligned}&\mathbf{U}_t \in \mathcal{U}(\mathbf{A}), \\ &\theta^t = \widetilde{\mu} \sup_{(\mathbf{H}^{a*}, \mathbf{N})} \|\mathbf{H}_t^a - \mathbf{H}^{a*}\|_{2,1} + \sigma C_U,\end{aligned} \quad (41)$$

where $\widetilde{\mu} = \widetilde{\mu}(\mathbf{A})$ and $C_U = \max_{t \geq 0} \|\mathbf{U}_t\|_{2,1}$.

B. Error Bound for an Individual Sample

To demonstrate the convergence of the proposed Radar-CEnet, we adapt the steps in [44] to suit our case. Since $\eta_{\theta_t, \mathbf{s}_r}$ is a sparse forcing function, we divide the indices of $\mathbf{H}^a$ into three parts. Let $\mathcal{E}_s$ represents the total number of non-zero row supports. $\mathcal{E}_r$ represents the set of known part non-zero row supports. $\mathcal{E}_r^c$ denotes the set of the rest non-zero row supports, which are estimated via the network. $\mathcal{E}^c$ denotes the index set of zero rows. The number of elements in those set are defined as $\mathcal{E}_s = E_s$, $\mathcal{E}_r = E_r$, $\mathcal{E}_r^c = E_s - E_r$ and $\mathcal{E}^c = E - E_s$.

To obtain information about group row-sparsity, we first define a new function $f(\mathbf{X})$:

$$f(\mathbf{X}) = \left[\|\mathbf{X}[1,:]\|_2, \|\mathbf{X}[2,:]\|_2, \cdots, \|\mathbf{X}[2G,:]\|_2 \right]^T, \quad (42)$$

where the function computes the ℓ_2-norm of each row of the matrix and combines these norm values into a column vector. For a sparse vector $\mathbf{b} = [b_1, b_2, \cdots, b_{2G}]^T \in \mathbb{R}^{2G}$, we have $f(\mathbf{b}[i]) = |b_i|$, $i \in [2G]$. Note that supp$(f(\mathbf{H}^a))$ can provide information about group row-sparsity of a given matrix $\mathbf{H}^a$.

To analyze the convergence of the Radar-CEnet network, we first prove that $\mathbf{H}_t^a$ has no false positive rows, which involves proving the following lemma.

Lemma 2: With $(\mathbf{H}^{a*}, \mathbf{Z}) \in \mathcal{H}(\beta, E_s, \sigma)$, as long as optimal parameters are used, we have

$$\mathbf{H}_t^a[i,:] = 0, \ \forall i \notin \mathcal{E}_s, \ \forall t, \quad (43)$$

where $\mathcal{E}_s = \text{supp}(f(\mathbf{H}^{a*}))$. This indicates that the rows not included in the set $\mathcal{E}_s$ can always be perfectly recovered. The proof can be found in Appendix A.

Next, we focus on the components in $\mathcal{E}_s$. Since $\mathcal{E}_s$ consists of the known non-zero row support set $\mathcal{E}_r$ and the unknown non-zero row supports $\mathcal{E}_r^c$, we first analyze these two cases separately and then combine the results to derive the recovery bound for the proposed Radar-CEnet.

For a single non-zero row in the matrix, namely an individual sample $i \in \mathcal{E}_r$, the Radar-CEnet in (35) gives

$$\begin{aligned}
&\mathbf{H}^a_{t+1}[i,:] \\
=&\eta_{\theta_t,\mathbf{s}_r}\big(\mathbf{H}^a_t[i,:] - (\mathbf{U}_t[:,i])^T\mathbf{A}(:,\mathcal{E}_r)(\mathbf{H}^a_{t+1}(\mathcal{E}_r,:) \\
&- \mathbf{H}^{a*}(\mathcal{E}_r,:)) + (\mathbf{U}_t[i,:])^T\mathbf{N}\big) \\
=&\mathbf{H}^a_t[i,:] - (\mathbf{U}_t[:,i])^T\mathbf{A}(:,\mathcal{E}_r)(\mathbf{H}^a_{t+1}(\mathcal{E}_r,:) - \mathbf{H}^{a*}(\mathcal{E}_r,:)) \\
&+ (\mathbf{U}_t[:,i])^T\mathbf{N} \\
=&\mathbf{H}^{a*}[i,:] - \sum_{\substack{j\in E_r,\\ j\neq i}} (\mathbf{U}_t[:,i])^T\mathbf{A}[:,j](\mathbf{H}^a_{t+1}[j,:] - \mathbf{H}^{a*}[j,:]) \\
&+ (\mathbf{U}_t[:,i])^T\mathbf{N}.
\end{aligned} \tag{44}$$

Then, we can obtain

$$\begin{aligned}
&\|\mathbf{H}^a_{t+1}[i,:] - \mathbf{H}^{a*}[i,:]\|_2 \\
\leq &\sum_{\substack{j\in E_r,\\ j\neq i}} (\mathbf{U}_t[:,i])^T\mathbf{A}[:,j]\|\mathbf{H}^a_{t+1}[j,:] - \mathbf{H}^{a*}[j,:]\|_2 \\
&+ \|(\mathbf{U}_t[:,i])^T\mathbf{N}\|_2 \\
\leq &\widetilde{\mu} \sum_{\substack{j\in E_r,\\ j\neq i}} \|\mathbf{H}^a_{t+1}[j,:] - \mathbf{H}^{a*}[j,:]\|_2 + (\mathbf{U}_t[:,i])^T\mathbf{N}.
\end{aligned} \tag{45}$$

Next, we consider the case when $i \in \mathcal{E}^c_r$:

$$\begin{aligned}
&\mathbf{H}^a_{t+1}[i,:] \\
=&\eta_{\theta_t,\mathbf{s}_r}\big(\mathbf{H}^a_t[i,:] - (\mathbf{U}_t[:,i])^T\mathbf{A}(:,\mathcal{E}^c_r)(\mathbf{H}^a_{t+1}(\mathcal{E}^c_r,:) \\
&- \mathbf{H}^{a*}(\mathcal{E}^c_r,:)) + (\mathbf{U}_t[:,i])^T\mathbf{N}\big) \\
\in&\mathbf{H}^a_t[i,:] - (\mathbf{U}_t[:,i])^T\mathbf{A}(:,\mathcal{E}^c_r)(\mathbf{H}^a_{t+1}(\mathcal{E}^c_r,:) - \mathbf{H}^{a*}(\mathcal{E}^c_r,:)) \\
&+ (\mathbf{U}_t[:,i])^T\mathbf{N} - \theta^t\partial\|\mathbf{H}^a_{t+1}[i,:]\|_2 \\
=&\mathbf{H}^{a*}[i,:] - \sum_{\substack{j\in E^c_r,\\ j\neq i}} (\mathbf{U}_t[:,i])^T\mathbf{A}[:,j](\mathbf{H}^a_{t+1}[j,:] - \mathbf{H}^{a*}[j,:]) \\
&+ (\mathbf{U}_t[:,i])^T\mathbf{N} - \theta^t\partial\|\mathbf{H}^a_{t+1}[i,:]\|_2,
\end{aligned} \tag{46}$$

where $\partial\|\cdot\|_2$ is the sub-gradient of $\mathbf{H}^a[i,:]$:

$$\partial\|\mathbf{H}^a[i,:]\|_2 = \begin{cases} \{\frac{\mathbf{H}^a[i,:]}{\|\mathbf{H}^a[i,:]\|_2}\}, & if\ \mathbf{H}^a[i,:] \neq \mathbf{0} \\ \{\mathbf{h}\in\mathbb{R}^K \mid \|\mathbf{h}\|_2 \leq 1\}, & if\ \mathbf{H}^a[i,:] = \mathbf{0} \end{cases} \tag{47}$$

where the ℓ_2-norm is smooth at nonzero points, thus it has a unique gradient. However, at zero, since the gradient of the ℓ_2-norm does not exist, we use the subgradient set to represent all possible directions. In this case, the subgradient set consists of all vectors with an ℓ_2-norm less than or equal to 1.

Then, we can obtain $\|\mathbf{H}^a_{t+1}[i,:] - \mathbf{H}^{a*}[i,:]\|_2$ when i belongs to the set without prior support information. Since $\|\partial\|\mathbf{H}^a_{t+1}[i,:]\|_2\|_2 \leq 1$, we can deduce:

$$\begin{aligned}
&\|\mathbf{H}^a_{t+1}[i,:] - \mathbf{H}^{a*}[i,:]\|_2 \\
\leq &\sum_{\substack{j\in E^c_r,\\ j\neq i}} (\mathbf{U}_t[:,i])^T\mathbf{A}[:,j]\|\mathbf{H}^a_{t+1}[j,:] - \mathbf{H}^{a*}[j,:]\|_2 \\
&+ \|(\mathbf{U}_t[:,i])^T\mathbf{N}\|_2 + \theta^t \\
\leq &\widetilde{\mu} \sum_{\substack{j\in E^c_r,\\ j\neq i}} \|\mathbf{H}^a_{t+1}[j,:] - \mathbf{H}^{a*}[j,:]\|_2 + (\mathbf{U}_t[:,i])^T\mathbf{N} + \theta^t.
\end{aligned} \tag{48}$$

So far, we have derived the error expressions for a single sample in both cases where the support is known and unknown. Next, we will extend this analysis to the entire sample set to obtain the recovery error bound.

C. Error Bound for Entire Sample Set

This subsection gives an upper bound of recovery error for the entire sample set. We first establish the $\ell_{2,1}$-norm of the error:

$$\begin{aligned}
&\|\mathbf{H}^a_{t+1} - \mathbf{H}^{a*}\|_{2,1} \\
=&\sum_{i\in E_r}\|\mathbf{H}^a_{t+1}[i,:] - \mathbf{H}^{a*}[i,:]\|_2 + \sum_{i\in E^c_r}\|\mathbf{H}^a_{t+1}[i,:] - \mathbf{H}^{a*}[i,:]\|_2 \\
\leq &\sum_{i\in E_r}\big(\widetilde{\mu}\sum_{\substack{j\in E_r,\\ j\neq i}}\|\mathbf{H}^a_{t+1}[j,:] - \mathbf{H}^{a*}[j,:]\|_2 + (\mathbf{U}_t[:,i])^T\mathbf{N}\big) + \\
&\sum_{i\in E^c_r}\big(\widetilde{\mu}\sum_{\substack{j\in E^c_r,\\ j\neq i}}\|\mathbf{H}^a_{t+1}[j,:] - \mathbf{H}^{a*}[j,:]\|_2 + (\mathbf{U}_t[:,i])^T\mathbf{N} + \theta^t\big).
\end{aligned} \tag{49}$$

After substituting the number of elements in each set, we can obtain:

$$\begin{aligned}
&\|\mathbf{H}^a_{t+1} - \mathbf{H}^{a*}\|_{2,1} \\
\leq&\widetilde{\mu}(E_r-1)\sum_{\substack{j\in E_r,\\ j\neq i}}\|\mathbf{H}^a_{t+1}[j,:] - \mathbf{H}^{a*}[j,:]\|_2 + \widetilde{\mu}(E_s - E_r - 1) \\
&\sum_{\substack{j\in E^c_r,\\ j\neq i}}\|\mathbf{H}^a_{t+1}[j,:] - \mathbf{H}^{a*}[j,:]\|_2 + \sigma C_U + (E_s - E_r)\theta^t.
\end{aligned} \tag{50}$$

Taking supremum over $\mathcal{H}(\beta, E_s, \sigma) \in (\mathbf{H}^{a*}, \mathbf{N})$ on both sides of (50), and $\theta^t = \widetilde{\mu}\sup_{(\mathbf{H}^{a*},\mathbf{N})}\|\mathbf{H}^a_t - \mathbf{H}^{a*}\|_{2,1} + \sigma C_U$. We can obtain

$$\begin{aligned}
&\sup_{(\mathbf{H}^{a*},\mathbf{N})}\|\mathbf{H}^a_{t+1} - \mathbf{H}^{a*}\|_{2,1} \\
\leq&\widetilde{\mu}\max\{E_s - 1, 2E_s - 2E_r - 1\}\sup_{(\mathbf{H}^{a*},\mathbf{N})}\|\mathbf{H}^a_t - \mathbf{H}^{a*}\|_{2,1} \\
&+ (E_s - E_r + 1)\sigma C_U.
\end{aligned} \tag{51}$$

By induction, we have

$$
\begin{aligned}
&\sup_{(\mathbf{H}^{a*},\mathbf{N})} \|\mathbf{H}^a_{t+1} - \mathbf{H}^{a*}\|_{2,1} \\
\leq&[\widetilde{\mu}\max\{E_s-1, 2E_s-2E_r-1\}]^{t+1}(E_s+1)\beta + (E_s-E_r \\
&+1)\sigma C_U \sum_{\tau=1}^{t+1}\left((\widetilde{\mu})^{\tau}(\max\{E_s-1, 2E_s-2E_r-1\})^{\tau}\right) \\
\leq&E_s\beta exp(-\alpha t) + A\sigma.
\end{aligned}
\tag{52}
$$

where $\alpha = -log(\widetilde{\mu}\max\{E_s-1, 2E_s-2E_r-1\})$ and $A = \frac{(E_s-E_r+1)C_U}{1-\widetilde{\mu}\max\{E_s-1,2E_s-2E_r-1\}}$. To promote the convergence of the network, the error bound should decrease with the iterations. Thus, we have

$$
\widetilde{\mu}\max\{E_s-1, 2E_s-2E_r-1\} < 1. \tag{53}
$$

This is equal to

$$
E_s < max\{1+1/\widetilde{\mu}, (1+1/\widetilde{\mu})/2 + E_r\}. \tag{54}
$$

The fact that $\|\mathbf{H}^a\|_F \leq \|\mathbf{H}^a\|_{2,1}$ for any matrix gives an upper bound of error. As long as $E_s < max\{1+1/\widetilde{\mu}, (1+1/\widetilde{\mu})/2+E_r\}$, we have

$$
\begin{aligned}
\sup_{(\mathbf{H}^{a*},\mathbf{N})} \|\mathbf{H}^a_{t+1} - \mathbf{H}^{a*}\|_F \leq &\sup_{(\mathbf{H}^{a*},\mathbf{N})} \|\mathbf{H}^a_{t+1} - \mathbf{H}^{a*}\|_{2,1} \\
\leq &E_s\beta exp(-\alpha t) + A\sigma.
\end{aligned}
\tag{55}
$$

Therefore, we complete the proof of Theorem 2.

Theorem 2 shows that the incorporation of prior information can significantly improve the estimation accuracy of the proposed algorithm, and this improvement is both intuitive and reasonable. In contrast, the ISTA-GS algorithm suffers from lower computational accuracy and exhibits sublinear convergence. To address this issue, LISTA-GS models the iterative process of ISTA-GS as a NN, introducing learnable parameters and optimizing them with training data, thereby accelerating the convergence speed of the algorithm. For the proof of convergence of LISTA-GS, refer to [47]. Compared to LISTA-GS, Radar-CENet further incorporates partial prior information, making the solution process more targeted, thereby significantly improving the estimation performance.

V. Numerical Results

In this section, we will futher analyze the discussion through simulations and compare the performance of the proposed scheme under different conditions. This section consists of two parts: angle estimation in the radar module and channel estimation in the communication module.

Uplink transmission frame structure: $T_s = 1\mu s$ and the number of pilots are $P_1 = 100$, $C_G = 16$. For MIMO Radar module: The transmitting and receiving arrays of the radar are equipped with $Z = 16$. There are three uncorrelated UEs in the V2X scenarios. For communication module: the mmWave frequency is 28GHz. The RSU is equipped with the number of antennas $N_{BS} = 64$ and $N_{RF} = 4$ RF chains. The number of OFDM subcarriers in the channel estimation process is set to $K = 64$.

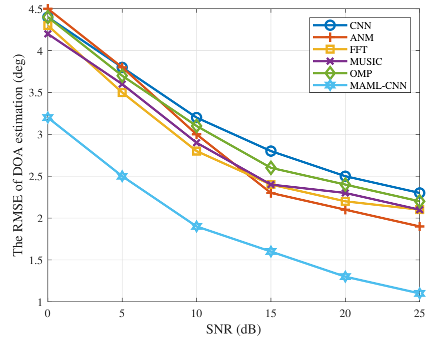

Fig. 6. DOA estimation performance with different SNRs.

A. Angle Estimation Performance of the Radar Module

In this subsection, we present the performance of the meta-learning-based angle estimation method for imperfect arrays. For the MAML-CNN network, the inner-task learning rate $\alpha = 0.001$, and the across-task learning rate $\beta = 0.01$. In the meta-learning process, the total number of tasks is 100, and 20 tasks are randomly selected from the total tasks for each meta-training iteration. Each set of meta-learning data contains a total of 200 samples, including both the training dataset and the testing dataset. The MAML-CNN algorithm program is implemented in a Python 3.7 environment with PyTorch 1.4.

The hyperparameters for the imperfect radar array are specified as follows: the maximum standard deviations of position, gain, and phase mismatches are 0.1, 0.3, and 0.15, respectively; the maximum mutual coupling effect is 0.03; and the maximum nonlinear effect is 1. An imperfection parameter scaling factor $\zeta \in [0.1, 1]$ is introduced to proportionally adjust these values, allowing us to evaluate system performance under different imperfection levels. The root mean square error (RMSE) is adopted as the performance metric:

$$
\text{RMSE} = \sqrt{\frac{1}{N_{sum}M}\|\hat{\boldsymbol{\theta}} - \boldsymbol{\theta}\|_2^2}, \tag{56}
$$

where N_{sum} is the number of simulation datas, and M is the number of targets.

Fig. 6 illustrates the RMSE performance comparison of various methods in DOA estimation with imperfect arrays under different SNR conditions. As shown in Fig. 6, the RMSE of all methods gradually decreases as the SNR increases, indicating that higher SNR contributes to improve accuracy in DOA estimation. ANM and OMP perform poorly at low SNR, but their performance gradually approaches that of the FFT and MUSIC methods under high SNR conditions. In comparison, the CNN method has a higher RMSE, making it the weakest performing method. This is due to the limited amount of data, which prevents the network from fully learning. The MAML-CNN method consistently performs the best across the entire SNR range, with a particularly significant advantage at low SNR, demonstrating its strong robustness in noisy environments.

In Fig. 7, the RMSE performance of different methods in DOA estimation is compared under varying imperfection

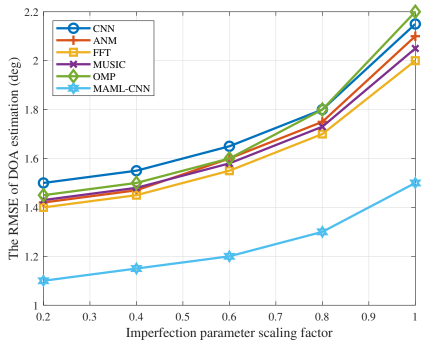

Fig. 7. DOA estimation performance with different imperfection parameter scaling factor.

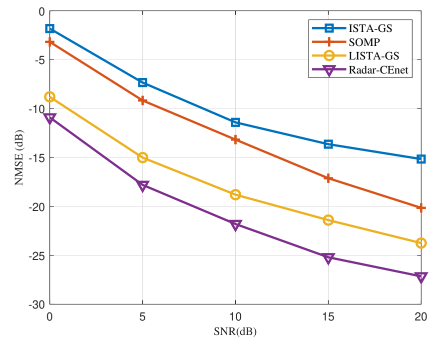

Fig. 8. NMSE performance versus different SNRs with $Q = 16$, $K = 64$ and $N_{BS} = 64$.

parameter scaling factor ζ. The results clearly demonstrate that as the imperfection parameter scaling factor increases, the RMSE of all methods exhibits a significant increase, indicating that the degree of array imperfection substantially impacts the accuracy of DOA estimation. The MAML-CNN method consistently performs the best across all ranges of imperfection parameter scaling factor, achieving the lowest RMSE, which demonstrates its strong robustness to array imperfections. Traditional methods such as MUSIC, FFT, OMP, and ANM exhibit similar performance when the imperfection parameter scaling factor is small. However, as the imperfection parameter scaling factor increases, their RMSE rises rapidly, and performance differences gradually become apparent. Notably, when the imperfection parameter scaling factor approaches 1, the MAML-CNN method maintains a relatively low RMSE, whereas the RMSE of other methods increases significantly, highlighting their limitations. This demonstrates that the MAML-CNN method offers superior adaptability and stability in addressing various levels of array imperfections.

B. Channel Estimation of the Communication Module

In the communication module's channel estimation process, the quantized angular grids are set as $G = 2N_{BS}$. During network training, the batch size is fixed at 128, and Radar-CEnet consists of $T_1 = 15$ layers. The training process employs Adam [48] to minimize the MSE loss function (32), with an initial learning rate of 0.001, which is adjusted in stages. If the loss function does not decrease after 100 iterations, the learning rate is reduced by a specific percentage. This reduction is applied three times, with the learning rate being multiplied by 0.5, 0.1, and 0.01, respectively. The NMSE is selected as the performance evaluation metric, and it is defined as follows

$$\mathrm{NMSE}(\hat{\mathbf{H}}, \mathbf{H})(\mathrm{dB}) = 10\log_{10}(\mathbb{E}(\frac{\|\hat{\mathbf{H}} - \mathbf{H}\|_{\mathrm{F}}^2}{\|\mathbf{H}\|_{\mathrm{F}}^2})). \tag{57}$$

The proposed Radar-CEnet is compared with the traditional CS algorithms ISTA-GS and SOMP [49], as well as the DL method LISTA-GS.

For ISTA-GS, LISTA-GS, and Radar-CEnet, the per-layer computational complexity is primarily determined by matrix multiplication. Specifically, for ISTA-GS, the computational complexity of each iteration is $O(4QN_{RF}GK)$. For LISTA-GS and Radar-CEnet, since the only difference between them lies in the soft-thresholding operation within each iteration, their per-layer computational complexity is the same, given by $O(4QN_{RF}GK + 4G^2K)$. The computational complexity of the baseline algorithm SOMP is $O(4LQN_{RF}GK)$. Although LISTA-GS and Radar-CEnet share the same computational complexity per iteration, Radar-CEnet incorporates prior information during the iterative process, thereby requiring fewer iterations in practice.

In Fig. 8, the NMSE performance of different algorithms under various SNR conditions is compared. As the SNR increases, the NMSE of all methods gradually decreases, indicating that the channel estimation accuracy improves with higher SNR. ISTA-GS shows a small decrease in NMSE, indicating its poorer performance. SOMP performs better than ISTA-GS, but still not as well as the learning-based methods. Radar-CEnet outperforms all other methods across all SNR values, indicating its higher accuracy in channel estimation. Particularly under low SNR conditions, its NMSE is significantly lower than that of the other methods. Radar-CEnet is able to fully utilize structured sparsity and prior information, leading to more efficient channel estimation.

In Fig. 9, the channel estimation performance of various methods is presented under different numbers of BS antennas. As shown in the figure, the estimation performance of all methods degrades as the number of antennas increases, indicating that larger antenna arrays pose greater challenges for accurate channel estimation. Among the evaluated algorithms, the iterative ISTA-GS performs the worst. The SOMP algorithm outperforms ISTA-GS but still lags behind learning-based approaches. LISTA-GS, as a deep unfolding version of ISTA-GS, improves estimation accuracy by automatically learning optimal parameters through end-to-end training. Radar-CEnet achieves the best performance among all methods. Built upon LISTA-GS, it further incorporates prior knowledge of sparse support, which effectively reduces the learning difficulty and significantly enhances the accuracy of channel estimation.

Fig. 10 illustrates the NMSE performance of different channel estimation algorithms under varying numbers of pilot

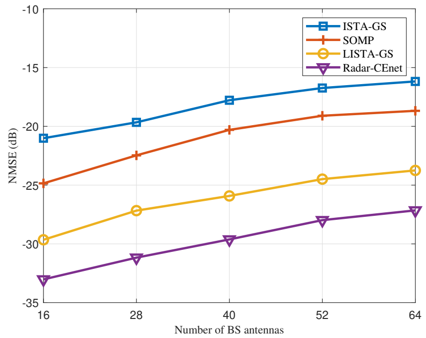

Fig. 9. NMSE performance under different numbers of BS antennas with $Q = 16$, $K = 64$ and $\mathrm{SNR} = 20dB$.

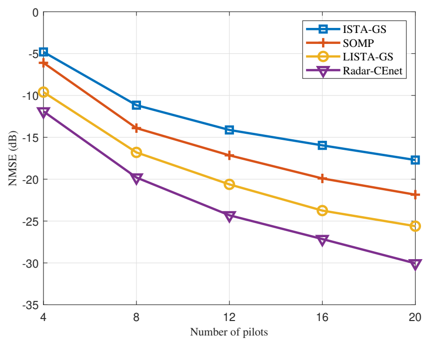

Fig. 10. NMSE performance versus the number of pilots with $\mathrm{SNR} = 20dB$, $K = 64$ and $N_{BS} = 64$.

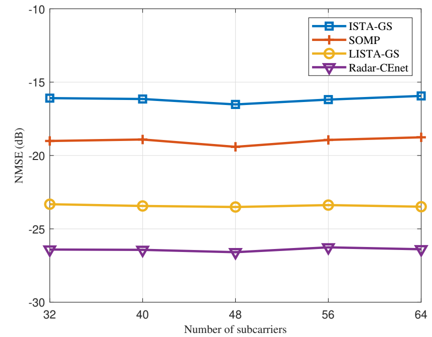

Fig. 11. NMSE performance versus the number of subcarriers with $\mathrm{SNR} = 20dB$, $Q = 16$ and $K = 64$.

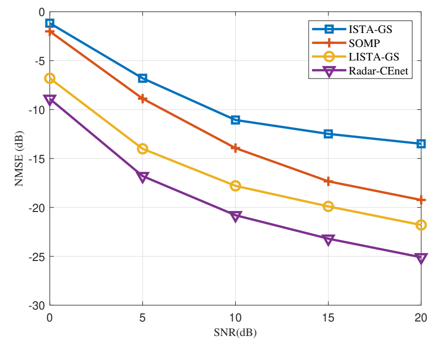

Fig. 12. NMSE performance comparison under varying SNRs on the CDL-E channel dataset.

signals. It can be observed that as the number of pilots increases, the NMSE of all methods gradually decreases, indicating that increasing the number of pilots helps improve the accuracy of channel estimation. In comparison, SOMP and ISTA-GS, as traditional compressed sensing algorithms, exhibit relatively poor performance, with ISTA-GS performing the worst. Among all methods, Radar-CEnet consistently achieves the lowest NMSE and demonstrates a more pronounced advantage in scenarios with fewer pilots. LISTA-GS ranks second, with performance significantly better than that of traditional algorithms. Overall, deep learning-based methods show clear superiority over traditional approaches in channel estimation tasks. It is worth noting that Radar-CEnet can effectively leverage structured sparsity and prior information, maintaining excellent estimation performance even in scenarios with limited pilot resources.

Fig. 11 illustrates the NMSE performance of various algorithms under different numbers of subcarriers. It can be observed that all methods exhibit relatively small performance variations across different subcarrier configurations, indicating strong robustness to changes in subcarrier settings. Radar-CEnet consistently achieves the best performance under all subcarrier configurations, attaining the lowest NMSE and demonstrating a significant performance advantage. This superiority mainly stems from the incorporation of angle information obtained from the radar module as prior knowledge, which enables partial identification of the sparse support in advance, significantly reduces the learning difficulty of the network, and further enhances the accuracy of channel estimation.

C. Simulation Results on the CDL-E Dataset

To comprehensively evaluate the performance of the proposed Radar-CEnet method under typical channel conditions, we generate CDL-E channel data based on the 3GPP TR 38.901 standard using the Sionna simulation platform, and conduct corresponding simulations under this channel model.

In the simulation experiments, the base station is equipped with 64 antennas and 4 RF chains. The number of sampling points in the angular domain is set to $2N_{BS} = 128$. A 28 GHz carrier frequency and 100 MHz system bandwidth are considered. We first employ the proposed MAML-CNN method to estimate the central angles of the propagation paths, and then determine the sparse support positions in the angle-domain sparse channel based on the estimated angle information. Based on the 3GPP CDL-E channel model parameters, we generate 56,000 channel samples, which are divided into 50,000 for training, 3,000 for validation, and 3,000 for testing. The training configuration of the Radar-CEnet network remains consistent with that described earlier.

Fig. 12 compares the NMSE performance of various methods under different SNRs using channel parameters from the 3GPP CDL-E model. It can be observed that the proposed Radar-CEnet method consistently achieves superior channel estimation performance on the CDL-E channel dataset. At an SNR of 20 dB, Radar-CEnet achieves approximately a 3 dB performance gain over the LISTA-GS algorithm, further validating the robustness of the proposed method under different channel statistical characteristics.

VI. Conclusions

In this paper, we propose a deep unfolding-based radar-assisted communication channel estimation method for V2X scenarios. To address the issue of limited data in imperfect MIMO radar arrays, we employ a meta-learning-based MAML-CNN approach to achieve high-precision angle estimation. The angle estimated by the radar module is transmitted to the communication module as prior knowledge for channel estimation. Leveraging this angle information, we can effectively identify the positions of some non-zero elements in the sparse channel. Based on this, we design a novel soft-thresholding shrinkage function and propose the Radar-CEnet algorithm based on deep unfolding. The novel soft-thresholding function retains the values at the positions of the non-zero elements while shrinking the values at other positions. Additionally, we rigorously prove the convergence of Radar-CEnet, providing a theoretical guarantee for the performance of the Radar-CEnet algorithm. Numerical results demonstrate that the proposed Radar-CEnet algorithm achieves lower channel estimation error compared to other competing algorithms.

Appendix A
The Proof of Lemma 2

We demonstrate that the no-false-positives property holds for the Radar-CEnet method. Specifically, $(\mathbf{H}^{a*}, \mathbf{Z}) \in \mathcal{H}(\beta, E_s, \sigma)$ and $\mathcal{E}_s = \text{supp}(g(\mathbf{X}^*))$, if (41) is satisfied, then $\mathbf{H}_t^a[i,:] = 0, \forall i \notin \mathcal{E}_s, \forall t$.

We first assume that when $t = 0$, $H_0^a = 0$ hold. Fixing t and assuming $\mathbf{H}_t^a = 0$, we can derive that

$$\begin{aligned}\mathbf{H}_{t+1}^a[i,:] &= \eta_{\theta_t, \mathbf{s}_r}(\mathbf{H}_t^a[i,:] + (\mathbf{U}_t[:i])^T(\mathbf{Y} - \mathbf{A}\mathbf{H}_t^a)) \\ &= \eta_{\theta_t, \mathbf{s}_r}\big(\mathbf{H}_t^a[i,:] - (\mathbf{U}_t[:i])^T \mathbf{A}(:, \mathcal{E}_r)(\mathbf{H}_t^a(\mathcal{E}_r,:) \\ &\quad - \mathbf{H}^{a*}(\mathcal{E}_r,:)) + (\mathbf{U}_t[:i])^T \mathbf{N}\big).\end{aligned} \tag{58}$$

Since $\mathbf{H}_t^a[i,:] = 0$, we only consider the remaining part.

$$\begin{aligned}&\|(\mathbf{U}_t[:i])^T(\mathbf{Y} - \mathbf{A}\mathbf{H}_t^a)\|_2 \\ &\le \sum_{j \in \mathcal{E}_s} |(\mathbf{U}_t[:i])^T \mathbf{A}[:,j]| \|\mathbf{H}_t^a[j,:] - \mathbf{H}^a[j,:]\|_2 \\ &\quad + \|(\mathbf{U}_t[:i])^T \mathbf{N}\|_2 \\ &\le \tilde{\mu} \|\mathbf{H}_t^a - \mathbf{H}^{a*}\|_{2,1} + \sigma C_U.\end{aligned} \tag{59}$$

Since $\theta_t = \widetilde{\mu} \sup_{(\mathbf{H}^{a*}, \mathbf{N})} \|\mathbf{H}_t^a - \mathbf{H}^{a*}\|_{2,1} + \sigma C_U$ and $\mathbf{U}_t \in \mathcal{U}(\mathbf{A})$. Therefore, for all $i \notin \mathcal{E}_s$, the following equality holds

$$\theta_t \ge \|(\mathbf{U}_t[:i])^T(\mathbf{Y} - \mathbf{A}\mathbf{H}_t^a)\|_2. \tag{60}$$

According to the definition of $\eta_{\theta_t, \mathbf{s}_r}$, $\|\mathbf{H}_{t+1}^a[i,:]\|_2 = 0, \forall i \notin \mathcal{E}_s$ can be obtained. Through induction, we can derive conclusion $\|\mathbf{H}_t^a[i,:]\|_2 = 0, \forall i \notin \mathcal{E}_s, \forall t$.

References

[1] J. Yang, X. Gong, B. Ai, and W. Chen, "A priori based deep unfolding method for mmwave channel estimation in MIMO radar aided V2X communications," in *ICC 2023-IEEE International Conference on Communications*. IEEE, 2023, pp. 2946–2951.

[2] K. Abboud, H. A. Omar, and W. Zhuang, "Interworking of DSRC and cellular network technologies for V2X communications: A survey," *IEEE transactions on vehicular technology*, vol. 65, no. 12, pp. 9457–9470, 2016.

[3] F. Liu, Y. Cui, C. Masouros, J. Xu, T. X. Han, Y. C. Eldar, and S. Buzzi, "Integrated sensing and communications: Toward dual-functional wireless networks for 6G and beyond," *IEEE journal on selected areas in communications*, vol. 40, no. 6, pp. 1728–1767, 2022.

[4] B. Ai, Y. Lu, Y. Fang, D. Niyato, R. He, W. Chen, J. Zhang, G. Ma, Y. Niu, and Z. Zhong, "6G-enabled smart railways," *arXiv preprint arXiv:2505.12946*, 2025.

[5] S. Huang, M. Zhang, Y. Gao, and Z. Feng, "MIMO radar aided mmwave time-varying channel estimation in MU-MIMO V2X communications," *IEEE Transactions on Wireless Communications*, vol. 20, no. 11, pp. 7581–7594, 2021.

[6] Z. Gao, C. Hu, L. Dai, and Z. Wang, "Channel estimation for millimeter-wave massive MIMO with hybrid precoding over frequency-selective fading channels," *IEEE Communications Letters*, vol. 20, no. 6, pp. 1259–1262, 2016.

[7] Z. Xiao, P. Xia, and X.-G. Xia, "Codebook design for millimeter-wave channel estimation with hybrid precoding structure," *IEEE Transactions on Wireless Communications*, vol. 16, no. 1, pp. 141–153, 2016.

[8] C. Hu, L. Dai, T. Mir, Z. Gao, and J. Fang, "Super-resolution channel estimation for mmwave massive MIMO with hybrid precoding," *IEEE Transactions on Vehicular Technology*, vol. 67, no. 9, pp. 8954–8958, 2018.

[9] X. Gao, L. Dai, S. Zhou, A. M. Sayeed, and L. Hanzo, "Wideband beamspace channel estimation for millimeter-wave MIMO systems relying on lens antenna arrays," *IEEE Transactions on Signal Processing*, vol. 67, no. 18, pp. 4809–4824, 2019.

[10] J. Lee, G.-T. Gil, and Y. H. Lee, "Channel estimation via orthogonal matching pursuit for hybrid MIMO systems in millimeter wave communications," *IEEE Transactions on Communications*, vol. 64, no. 6, pp. 2370–2386, 2016.

[11] C. Huang, L. Liu, C. Yuen, and S. Sun, "Iterative channel estimation using LSE and sparse message passing for mmwave mimo systems," *IEEE Transactions on signal processing*, vol. 67, no. 1, pp. 245–259, 2018.

[12] W. Li, W. Chen, S. Wang, Y. Zhang, M. Matthaiou, and B. Ai, "AI-driven mobility management for high-speed railway communications: compressed measurements and proactive handover," *IEEE Vehicular Technology Magazine*, 2025.

[13] Y. Cheng, W. Chen, T. Hou, G. Y. Li, and B. Ai, "Learning rate-compatible linear block codes: An auto-encoder based approach," *IEEE Transactions on Vehicular Technology*, 2024.

[14] Y. Guo, W. Chen, F. Sun, J. Cheng, M. Matthaiou, and B. Ai, "Deep learning for CSI feedback: One-sided model and joint multi-module learning perspectives," *IEEE Communications Magazine*, 2024.

[15] X. Gong, W. Chen, B. Ai, and G. Leus, "Deep-learning-aided alternating least squares for tensor CP decomposition and its application to massive MIMO channel estimation," *IEEE Transactions on Communications*, 2024.

[16] M. Soltani, V. Pourahmadi, A. Mirzaei, and H. Sheikhzadeh, "Deep learning-based channel estimation," *IEEE Communications Letters*, vol. 23, no. 4, pp. 652–655, 2019.

[17] P. Dong, H. Zhang, G. Y. Li, I. S. Gaspar, and N. NaderiAlizadeh, "Deep CNN-based channel estimation for mmwave massive MIMO systems," *IEEE Journal of Selected Topics in Signal Processing*, vol. 13, no. 5, pp. 989–1000, 2019.

[18] J. Yang, B. Ai, W. Chen, S. Yang, G. Shi, N. Wang, and C. Yuen, "Deep learning-based near-field wideband channel estimation: A joint LISTA-CP approach," *IEEE Transactions on Vehicular Technology*, 2025.

[19] W. Chen, W. Wan, S. Wang, P. Sun, G. Y. Li, and B. Ai, "CSI-PPPNet: A one-sided one-for-all deep learning framework for massive MIMO CSI feedback," *IEEE Transactions on Wireless Communications*, vol. 23, no. 7, pp. 7599–7611, 2023.

[20] J. Yang, B. Ai, W. Chen, N. Wang, S. Yang, and C. Yuen, "Deep unfolding-based near-field channel estimation for 6G communications," *IEEE Transactions on Vehicular Technology*, 2025.

[21] X. Wei, C. Hu, and L. Dai, "Deep learning for beamspace channel estimation in millimeter-wave massive MIMO systems," *IEEE Transactions on Communications*, vol. 69, no. 1, pp. 182–193, 2020.

[22] W. Jin, H. He, C.-K. Wen, S. Jin, and G. Y. Li, "Adaptive channel estimation based on model-driven deep learning for wideband mmwave systems," in *2021 IEEE Global Communications Conference (GLOBECOM)*. IEEE, 2021, pp. 1–6.

[23] Z. Wei, F. Liu, C. Masouros, N. Su, and A. P. Petropulu, "Toward multi-functional 6G wireless networks: Integrating sensing, communication, and security," *IEEE Communications Magazine*, vol. 60, no. 4, pp. 65–71, 2022.

[24] X. Gan, C. Huang, Z. Yang, C. Zhong, X. Chen, Z. Zhang, Q. Guo, C. Yuen, and M. Debbah, "Bayesian learning for double-RIS aided ISAC systems with superimposed pilots and data," *IEEE Journal of Selected Topics in Signal Processing*, 2024.

[25] Y. Chen, H. Hua, J. Xu, and D. W. K. Ng, "ISAC meets SWIPT: Multi-functional wireless systems integrating sensing, communication, and powering," *IEEE Transactions on Wireless Communications*, 2024.

[26] J. A. Zhang, F. Liu, C. Masouros, R. W. Heath, Z. Feng, L. Zheng, and A. Petropulu, "An overview of signal processing techniques for joint communication and radar sensing," *IEEE Journal of Selected Topics in Signal Processing*, vol. 15, no. 6, pp. 1295–1315, 2021.

[27] F. Liu, C. Masouros, A. P. Petropulu, H. Griffiths, and L. Hanzo, "Joint radar and communication design: Applications, state-of-the-art, and the road ahead," *IEEE Transactions on Communications*, vol. 68, no. 6, pp. 3834–3862, 2020.

[28] L. Li, M. Zhu, S. Xia, and T.-H. Chang, "Downlink CSI recovery in massive mimo systems by proactive sensing," *IEEE Wireless Communications Letters*, vol. 12, no. 3, pp. 406–410, 2022.

[29] Z. Huang, K. Wang, A. Liu, Y. Cai, R. Du, and T. X. Han, "Joint pilot optimization, target detection and channel estimation for integrated sensing and communication systems," *IEEE Transactions on Wireless Communications*, vol. 21, no. 12, pp. 10 351–10 365, 2022.

[30] Z. Ren, L. Qiu, J. Xu, and D. W. K. Ng, "Sensing-assisted sparse channel recovery for massive antenna systems," *IEEE Transactions on Vehicular Technology*, 2024.

[31] X. Chen, Z. Feng, Z. Wei, X. Yuan, P. Zhang, J. A. Zhang, and H. Yang, "Multiple signal classification based joint communication and sensing system," *IEEE Transactions on Wireless Communications*, vol. 22, no. 10, pp. 6504–6517, 2023.

[32] X. Gong, W. Chen, L. Sun, J. Chen, and B. Ai, "An ESPRIT-based supervised channel estimation method using tensor train decomposition for mmwave 3-D MIMO-OFDM systems," *IEEE Transactions on Signal Processing*, vol. 71, pp. 555–570, 2023.

[33] W. S. Leite and R. C. de Lamare, "List-based OMP and an enhanced model for DOA estimation with nonuniform arrays," *IEEE Transactions on Aerospace and Electronic Systems*, vol. 57, no. 6, pp. 4457–4464, 2021.

[34] A. M. Ahmed, U. S. K. M. Thanthrige, A. El Gamal, and A. Sezgin, "Deep learning for doa estimation in mimo radar systems via emulation of large antenna arrays," *IEEE Communications Letters*, vol. 25, no. 5, pp. 1559–1563, 2021.

[35] Y. Ma, Y. Zeng, and S. Sun, "A deep learning based super resolution doa estimator with single snapshot mimo radar data," *IEEE Transactions on Vehicular Technology*, vol. 71, no. 4, pp. 4142–4155, 2022.

[36] S. Zheng, Z. Yang, W. Shen, L. Zhang, J. Zhu, Z. Zhao, and X. Yang, "Deep learning-based doa estimation," *IEEE Transactions on Cognitive Communications and Networking*, vol. 10, no. 3, pp. 819–835, 2024.

[37] S. Liu, Z. Zhang, and Y. Guo, "2-D doa estimation with imperfect l-shaped array using active calibration," *IEEE Communications Letters*, vol. 25, no. 4, pp. 1178–1182, 2020.

[38] Z.-M. Liu and Y.-Y. Zhou, "A unified framework and sparse bayesian perspective for direction-of-arrival estimation in the presence of array imperfections," *IEEE Transactions on Signal Processing*, vol. 61, no. 15, pp. 3786–3798, 2013.

[39] J. Cong, X. Wang, M. Huang, and L. Wan, "Robust DOA estimation method for MIMO radar via deep neural networks," *IEEE Sensors Journal*, vol. 21, no. 6, pp. 7498–7507, 2020.

[40] P. Chen, Z. Chen, L. Liu, Y. Chen, and X. Wang, "SDOA-Net: An efficient deep learning-based DOA estimation network for imperfect array," *IEEE Transactions on Instrumentation and Measurement*, 2024.

[41] X. Ma, Z. Gao, F. Gao, and M. Di Renzo, "Model-driven deep learning based channel estimation and feedback for millimeter-wave massive hybrid MIMO systems," *IEEE Journal on Selected Areas in Communications*, vol. 39, no. 8, pp. 2388–2406, 2021.

[42] M. Ke, Z. Gao, Y. Wu, X. Gao, and R. Schober, "Compressive sensing-based adaptive active user detection and channel estimation: Massive access meets massive MIMO," *IEEE transactions on signal processing*, vol. 68, pp. 764–779, 2020.

[43] Y. Shi, S. Xia, Y. Zhou, and Y. Shi, "Sparse signal processing for massive device connectivity via deep learning," in *2020 IEEE international conference on communications workshops (ICC Workshops)*. IEEE, 2020, pp. 1–6.

[44] Y. Bai, W. Chen, B. Ai, Z. Zhong, and I. J. Wassell, "Prior information aided deep learning method for grant-free NOMA in mMTC," *IEEE Journal on Selected Areas in Communications*, vol. 40, no. 1, pp. 112–126, 2021.

[45] B. Xin, Y. Wang, W. Gao, D. Wipf, and B. Wang, "Maximal sparsity with deep networks?" *Advances in Neural Information Processing Systems*, vol. 29, 2016.

[46] X. Chen, J. Liu, Z. Wang, and W. Yin, "Theoretical linear convergence of unfolded ISTA and its practical weights and thresholds," *Advances in Neural Information Processing Systems*, vol. 31, 2018.

[47] Y. Shi, H. Choi, Y. Shi, and Y. Zhou, "Algorithm unrolling for massive access via deep neural networks with theoretical guarantee," *IEEE Transactions on Wireless Communications*, vol. 21, no. 2, pp. 945–959, 2021.

[48] D. P. Kingma and J. Ba, "Adam: A method for stochastic optimization," *arXiv preprint arXiv:1412.6980*, 2014.

[49] X. Ma, Z. Gao, F. Gao, and M. Di Renzo, "Model-driven deep learning based channel estimation and feedback for millimeter-wave massive hybrid MIMO systems," *IEEE Journal on Selected Areas in Communications*, vol. 39, no. 8, pp. 2388–2406, 2021.